mater.scichina.com link.springer.com

Published online 10 July 2020 | https://doi.org/10.1007/s40843-020-1360-8
Sci China Mater 2021, 64(1): 128–136

Carbon-CeO_2 interface confinement enhances the chemical stability of Pt nanocatalyst for catalytic oxidation reactions

Changjin Xu[1], Yue Zhang[1], Jing Chen[2], Song Li[1*], Ya-Wen Zhang[3] and Gaowu Qin[1,4]

ABSTRACT **Noble metals are downsized to nano-/subnano-scale to improve their catalytic activity and atom-economy. However, the stabilities in chemical state and catalytic performance of these nanocatalysts often suffer during harsh conditions. For Pt nanoparticles (NPs) supported on CeO_2, activated oxygen diffused from the support over-stabilizes the active sites of Pt, degrading its performance at mild temperature. In this work, Pt nanocatalysts with unique structure of triple-junction are synthesized by selectively growing Pt NPs on the carbon-CeO_2 interface. Impressively, the Pt NPs exhibit much enhanced catalytic stability and high activity for CO oxidation at mild temperature. The enhancement is attributed to electron donation from graphitized carbon and the confinement effect from the high-density nanopores of the CeO_2 support. The triple-junction of Pt-C-CeO_2, combining the merits of CeO_2 for activating O_2 and electron donating capability of carbon, provides new inspiration to the fabrication of high-performance nanocatalysts.**

Keywords: catalyst stability, Pt nanocatalyst, interface confinement

INTRODUCTION

Nanometals dispersed on oxide supports play crucial roles in a wide range of chemical reactions covering energy conversion, chemical production, and pollution elimination [1–5]. Performance instability of the deliberately fabricated nanostructures is a major hurdle to their large-scale applications in industry [6]. Two mechanisms have been essentially identified for the progressive degradation of nanocatalysts, i.e., (i) sintering of the metal nanoparticles (NPs) driven by the reduction in the surface energy [7,8], and (ii) variation of their chemical states that determine the adsorption/desorption of intermediates [9]. To cure the former, thermodynamic or kinetic countermeasures have been taken, including strengthening the adhesion metal on the support surface [10,11], building energy barriers for atomic migration [12,13], or confining the NPs inside limited space [14,15]. However, catalysts still suffer from additional instability in chemical states, especially under oxidative conditions.

To improve the catalytic activity, the binding strength of intermediates on active sites is intentionally adjusted *via* manipulation of the electronic structure of nanometals, by means of alloying [16] or changing support [17,18]. In particular, the electronic metal-support interaction (EMSI) is emphasized since its discovery on the Pt/CeO_2 [19,20]. To practice the EMSI effect, reducible oxides are used as support [2,21–24] so that the charge transfer across the interface promotes the nanocatalyst activity. A side-effect of the interaction is that the chemical states of nanometal in direct contact with the reducible oxide are prone to change. For example, metallic Pt rather than PtO_x has been identified as the active site for CO oxidation at mild temperatures (below 100°C) [25,26]. However, the metallic Pt is easily oxidized to inactive PtO_x under mild condition through oxygen diffusion from the reducible oxide support [27]. As a consequence, Pt NPs decay rapidly [9] and the CO oxidation

[1] Key Lab for Anisotropy and Texture of Materials (MoE), School of Materials Science and Engineering, Northeastern University, Shenyang 110819, China
[2] Institute of Microscale Optoelectronics (IMO), Shenzhen University, Shenzhen 518060, China
[3] Beijing National Laboratory for Molecular Sciences, State Key Laboratory of Rare Earth Materials Chemistry and Applications, PKU-HKU Joint Laboratory in Rare Earth Materials and Bioinorganic Chemistry, Peking University, Beijing 100871, China
[4] Research Center for Metallic Wires, Northeastern University, Shenyang 110819, China
* Corresponding author (email: lis@atm.neu.edu.cn)

must be performed at elevated temperatures where PtO_x is active. Therefore, further efforts should be contributed to design novel nanostructures that can simultaneously maintain the electronic and structural stability under reaction conditions.

Currently, metal-organic frameworks (MOFs) are attracting intensive attention due to their exotic properties such as large specific surface areas, ordered structure, high porosity, and large cavity size, finding wide applications in the fields including gas sensors, drug delivery, chemical separations, and heterogeneous catalysis [28–32]. Also, MOFs serve as platform materials for constructing nanoarchitectures [33–36]. The pyrolysis of MOF precursors under inert gas generates carbon modified oxides, providing a robust route to interfere the metal-support interaction [37]. Hopefully, the electronic and structural stability of noble metal NPs could be simultaneously achieved *via* this strategy.

In this work, we report the stabilization of Pt NPs by carbonizing the Pt-CeO_2 interface that could be achieved by pyrolysis of Ce-MOFs. The preparation involves the following steps: an octahedron-shaped Ce-BDC MOFs is firstly prepared through a solvothermal route by using formic acid as the structure-modulator agent. After thermal carbonization under inert atmosphere, the MOFs are converted into porous CeO_2 with the surface partially covered by carbon. After loading Pt NPs, the surface carbon fixes the valance state of Pt by serving as an electron reservoir [38]. And the high-density mesoporous structure in CeO_2-C restricts the diffusion of Pt. Our results show that the three-phase junction derived from MOFs conversion and selective deposition represents an effective strategy that enables simultaneous stabilization of atomic and electronic structure of supported noble metal NPs.

EXPERIMENTAL SECTION

Synthesis of Ce-BDC MOFs

Ce-BDC MOFs precursor was prepared by the following procedure. Firstly, 35.4 mg of 1,4-benzenedicarboxylic acid (H_2BDC) was dissolved into 3 mL of *N*,*N*-dimethylformamide (DMF)-formic acid (FA) mixed solution (V_{DMF}/V_{FA}=4:1) and sonicated for 10 min. Subsequently, 1 mL of $(NH_4)_2{\cdot}Ce(NO_3)_4$ (0.3 mol L^{-1}) aqueous solution was dropwise added into the above mixture. The resulting mixture was sealed in a vial and then reacted at 60°C for 2 h. The precipitates were separated by centrifugation, washed with DMF and acetone for three times, and finally dried at 60°C overnight in vacuum.

Synthesis of CeO_2 supports

The carbon-covered CeO_2-C with high-density nanopores was prepared by calcinating the Ce-BDC MOFs precursor at 600°C for 4 h in Ar atmosphere. For comparison, carbon-free CeO_2 support (denoted as CeO_2-P) also with high-density nanopores was achieved by calcinating the Ce-BDC MOFs precursor at 400°C for 4 h in a muffle furnace under the air atmosphere.

Synthesis of Pt/CeO_2 catalyst

In this work, Pt/CeO_2 catalysts were prepared *via* a surface redox reaction between Pt^{4+} and Ce^{3+}. Typical synthesis procedures are as follows: the as-synthesized CeO_2-C powers were dissolved in 100 mL of aqueous solution and then sonicated for 30 min. Then, a stoichiometric amount of chloroplatinic acid was added and the above solution was stirred for 2 h to reach adsorption equilibrium. Next, the pH of the above mixed solution was adjusted to about 8 with NaOH aqueous solution. Then, the suspension was held at 90°C for 4 h under vigorous magnetic stirring. Subsequently, the obtained precipitates were separated by centrifugation, washed, and then dried in vacuum to get powders. Finally, the powders were heated at 400°C for 2 h in the H_2 flow, which yielded the Pt/CeO_2-C catalyst. Meanwhile, the Pt/CeO_2-P catalyst was also prepared by the same procedure as that for Pt/CeO_2-C catalyst.

RESULTS AND DISCUSSION

Synthesis of Pt/CeO_2 nanocatalysts

A schematic of the synthesis process of Pt NPs supported on porous CeO_2 with and without surface carbon modification is depicted in Fig. 1a. First, the octahedral Ce-BDC MOFs hydrothermally grew in a solution containing Ce^{4+}, DMF, and H_2BDC. The carbon species in the Ce-BDC MOFs could be thoroughly removed by calcinating the MOFs in air (CeO_2-P route) or could be residually left on the surface to modify the physiochemical properties of CeO_2 when calcined in Ar (CeO_2-C route). Subsequently, Pt NPs were impregnated by spontaneous surface reaction to form the Pt/CeO_2 catalyst [22]. As shown in Fig. 1b, the as-prepared Ce-BDC MOFs present an octahedral shape with a smooth surface and an average size of 150 nm. After calcination, nanopores of high-density and uniform distribution in CeO_2-P (Fig. 1c) and the CeO_2-C (Fig. 1d) samples were prepared. Furthermore, the as-prepared Ce-BDC MOFs exhibit good structural stability to prevent structural collapse during the calcination (Fig. S1) and their surfaces are partially covered by carbon layer of

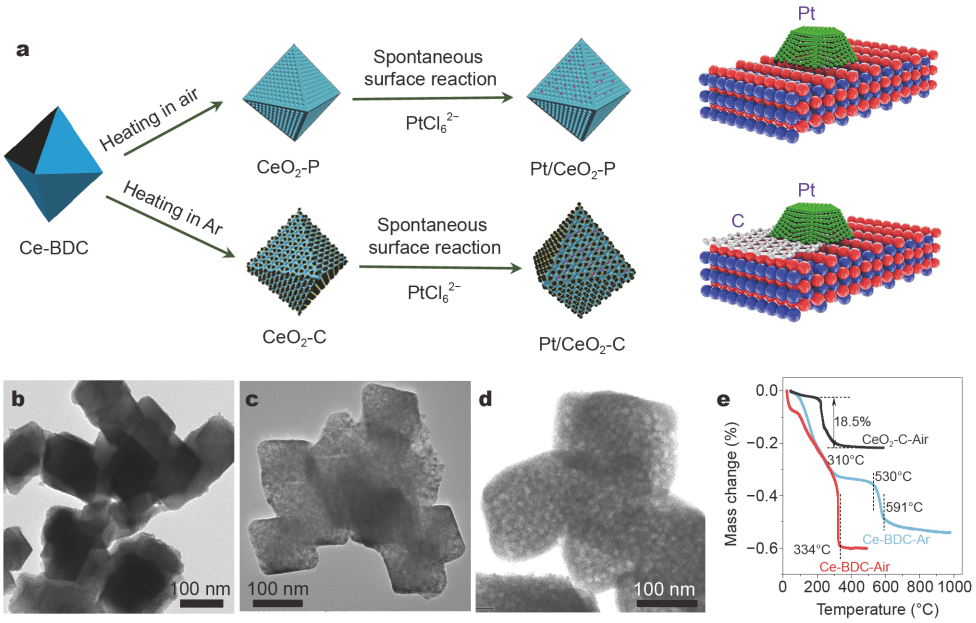

Figure 1 (a) Scheme for preparation of porous CeO_2 support by an MOF-assisted strategy. TEM images of Ce-BDC MOFs (b), CeO_2-P (c), and CeO_2-C (d). (e) TG curves.

~1 nm thickness (see high resolution transmission electron microscopy (HRTEM) images in Fig. S2).

The heating temperatures for converting Ce-BDC MOFs into porous CeO_2 in the two kinds of atmospheres were determined from thermogravimetric (TG) analysis since different reactions were involved. As shown in Fig. 1e, thermal decomposition of Ce-BDC MOFs proceeds *via* a stepwise pathway. The first weight loss below 310°C is assigned to the removal of adsorbed water molecules and DMF solvent [39]. The second weight loss above 310°C corresponds to the conversion from Ce-BDC MOFs to cerium oxide [40]. It is worth noting that the temperature for complete decomposition of the Ce-BDC MOFs is about 334°C in air and 591°C in Ar flow, respectively. Therefore, in this work, we chose 400°C in air and 600°C in Ar as the calcination temperatures to simultaneously ensure complete decomposition of Ce-BDC MOFs and minimize/avoid the sintering of the product. In addition, the TG curve in air shows that carbon stays on the CeO_2 surface before 200°C and the content of carbon in CeO_2-C is approximate 18.5 wt%. It is thus believed that the carbon in the Pt/CeO_2-C stays unchanged in the process of CO oxidation where the operating temperature is far below 200°C. Thus, the catalyst maintains its structural stability during the catalysis since the reaction temperature is lower than the calcination temperature. Moreover, the CeO_2-C and CeO_2-P are not different in nature except the former has a smaller CeO_2 grain size owing to the confinement of carbon, as evidenced later by widening of X-ray diffraction (XRD) peaks (Fig. S3).

Spontaneous redox reaction between the surface Ce^{3+} and adsorbed Pt^{4+} ions was used to guide the growth of Pt NPs on the CeO_2 surface. The electronic states of Pt NPs prepared by this method are strongly influenced by the interaction with the support due to the high-quality interface [22,41]. The high-angle annular dark-field scanning transmission electron microscopy (HAADF-STEM) images (Fig. 2) reveal that the octahedral morphology of CeO_2 was retained well after impregnating 2 wt% of Pt NPs; and no large Pt NPs were found on the surface. Element mapping by energy dispersive X-ray spectroscopy (EDX, Fig. 2a_1, b_1) shows that the Pt NPs are homogeneously distributed in the nanopores of MOFs-derived CeO_2. The average sizes of these Pt NPs on the Pt/CeO_2-C (Fig. 2a_2) and Pt/CeO_2-P (Fig. 2b_2) are 3.1 and 3.5 nm, respectively, in agreement with the results calculated by CO pulse chemisorption (Table S1). And the Pt NPs get in close contact with CeO_2, which features the interfacial growth of Pt by surface redox reaction. The Pt NPs grown on CeO_2-C are smaller because these NPs experience a stronger binding force from the support. Importantly, Pt NPs in the Pt/CeO_2-C sample are found homogeneously sitting at the carbon-ceria interface to form the Pt-CeO_2-C triple junctions, as shown in Fig. 2 and sketched in Fig. 1a. Such a unique structure results

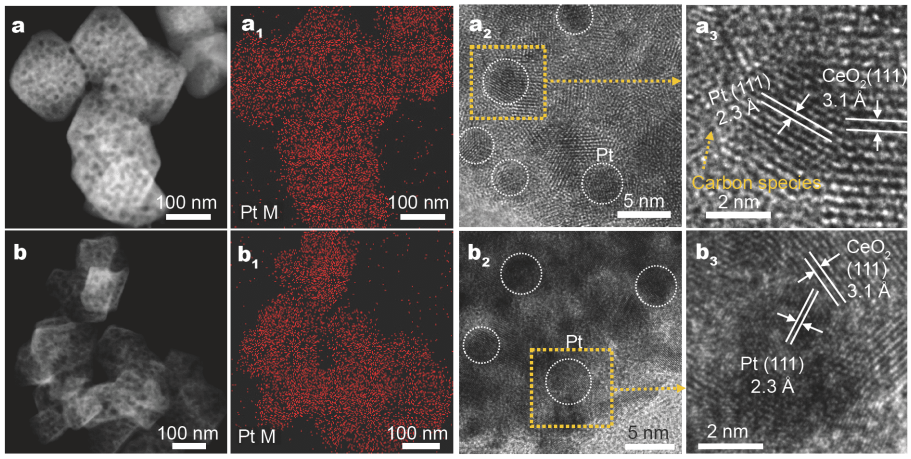

Figure 2 HAADF-STEM, TEM-EDX mapping and HRTEM images of Pt/CeO_2-C (a, a_1–a_3), and Pt/CeO_2-P (b, b_1–b_3), respectively. The crystal lattice fringes d=0.31 and 0.23 nm are attributed to (111) facets of CeO_2 and (111) planes of Pt, respectively. The white dash circles mark the Pt NPs.

from the site selective growth of Pt that is driven by the carbon-enhanced reduction ability of Ce^{3+}. Higher concentration of Ce^{3+} or oxygen vacancies in the CeO_2 results in less oxidative environment (Fig. S4). It is believed that the neighboring carbon regulates the interfaces between Pt NPs and CeO_2 and enhances the stability of the electronic structure of Pt NPs [42].

Catalytic performance

Considering the fine distribution of Pt NPs and the unique structure of the carbonized Pt/CeO_2-C, their catalytic properties were investigated through CO oxidation. Fig. 3a shows the conversion of CO as a function of temperature on catalysts of the same mass. The CeO_2-C support exhibits virtually no catalytic activity within the temperature range of 30–120°C. With the incorporation of Pt NPs into the mesoporous CeO_2 supports, the conversion of CO has a great increase and Pt/CeO_2-C presents a better activity than Pt/CeO_2-P in the temperature range of 30–90°C, confirming the importance of carbon

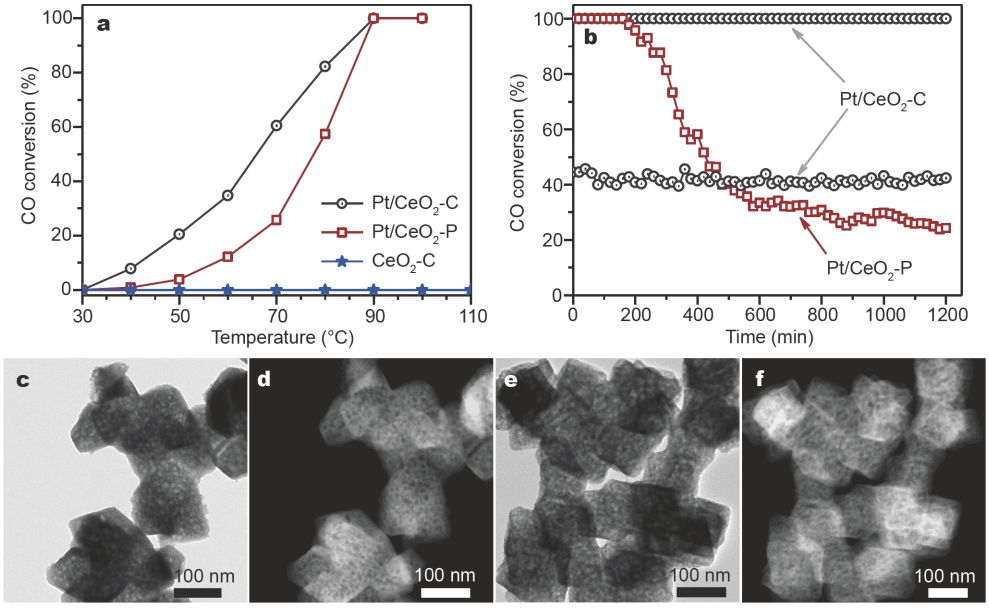

Figure 3 Catalytic performance of the Pt/CeO_2 catalysts. (a) CO conversion as function of reaction temperature. (b) CO conversion for stability test at 90°C (mass of catalysts: 70 mg for both catalysts and 25 mg for Pt/CeO_2-C to lower the CO conversion). TEM (c, e) and HAADF-STEM (d, f) images of the Pt/CeO_2-C (c, d) and Pt/CeO_2-P (e,f) catalysts after 20 h stability test.

species for improving the catalytic activity. Both samples reach a full conversion of CO at 90°C. However, the two catalysts exhibit different turnover frequencies (TOFs), 2.19×10^{-2} s^{-1} for the Pt/CeO_2-C and 0.58×10^{-2} s^{-1} for the Pt/CeO_2-P, respectively, which were calculated according to the loadings and dispersions of Pt (Table S1). The carbon in the Pt/CeO_2 junction position significantly enhances the activity of the Pt/CeO_2-C with a TOF four times higher than that of the Pt/CeO_2-P catalyst.

The long-term stabilities of the as-synthesized Pt nanocatalysts for the CO oxidation were tested at a complete and less than half conversion, as demonstrated in Fig. 3b. The CO conversion over the Pt/CeO_2-P maintained at 100% for about 3 h and then rapidly decreased. After continuous stability test for 20 h, CO conversion over the Pt/CeO_2-P decreased to about 25%. In contrast, the complete conversion of CO on the Pt/CeO_2-C catalyst did not decay for over 20 h, even at a higher temperature of 150°C (Fig. S5). Particularly, exceptionally high stability was observed under lower conversion (~43%) condition operated at a kinetics-control region (Fig. 3b).

When performed for catalysis, the nanometals tend to deactivate either by sintering of the particles [43,44] or by loss of valance electrons [45]. The acquired TEM/HAADF-STEM images of Pt/CeO_2 catalysts after stability test (Fig. 3c–f) show no obvious aggregation/growth of Pt NPs, implying the hindering effect of porous structure of the support on metal growth [15]. Thus, the activity decay of the Pt/CeO_2-P catalyst due to nanoparticle growth can be excluded. Over Pt/CeO_2 catalysts, a Mars-van Krevelen reaction mechanism is recommended where CO adsorbed Pt^0 reacts with active lattice oxygen species on the CeO_2 [1]. However, at high reaction temperatures, the main active sites for CO oxidation of Pt^0 are vulnerable to be oxidized, which could over-stabilize their surface lattice oxygen, losing catalytic reactivity progressively [9,26,46–48]. In this work, the performance stability of the Pt/CeO_2-C catalyst is enhanced because the surface carbon provides extra electrons suppressing the oxidation of Pt NPs.

Chemical states of Pt/CeO_2 nanocatalysts

We further characterized the electronic structure of the Pt of Pt/CeO_2 catalysts using X-ray photoelectron spectroscopy (XPS) to correlate with their stability performance. Fig. 4 shows two distinguishable peaks that can be assigned to Pt $4f_{5/2}$ and Pt $4f_{7/2}$. Through the deconvolution of Pt 4f peaks, constituent insights such as oxidation states and charge distributions can be obtained from the

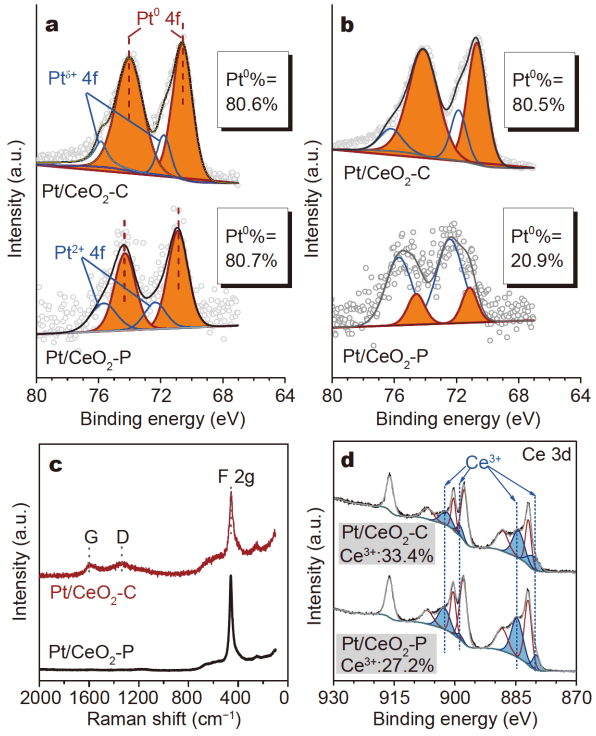

Figure 4 XPS spectra of Pt 4f peak of the as-prepared fresh Pt/CeO_2 catalysts (a) and after the 20 h stability test (b). The ratios of Pt^0 in the catalysts are displayed. Raman spectra (c) and Ce 3d XPS spectra (d) of the as-prepared Pt/CeO_2 catalysts.

core-level energy shifts of the surface Pt species relative to the bulk. The relative composition of the metallic Pt in all Pt species was estimated based on the deconvoluted peak areas in Fig. 4a, b. The results showed that both fresh Pt/CeO_2 catalysts carried about 80% Pt^0, but only the Pt/CeO_2-C reserved most of its metallic Pt^0 after running at 150°C for 20 h (Fig. S6). Therefore, it is reasonable to infer that the deactivation of Pt/CeO_2-P catalyst is caused by losing the valance electrons since the Pt^0 species serve as the main active sites for catalyzing the CO oxidation at mild temperature [1,25,49]. To be more specific, the unique tri-junction structure of Pt-carbon-CeO_2 in the Pt/CeO_2-C retards the oxidation of Pt by donating electrons to compensate the electron loss of Pt species. Correspondingly, a shift of the Pt binding energy towards the lowest position (70.6 eV) is observed on the Pt/CeO_2-C, indicating a strong EMSI induced by carbonizing Pt-CeO_2 interfaces [5].

The partial graphitization of the Pt/CeO_2-C surface was further confirmed by Raman spectra in Fig. 4c. The two remarkable peaks at 1348 and 1598 cm^{-1} correspond to the typical D and G bands, respectively [50]. The high

ratio of D to G band intensities (I_D/I_G, 1.02) suggests that the carbon layer is defective [51]. The defects in carbon, by breaking the lattice symmetry, favor both anchoring the metal NPs and generating an electronic interaction with Pt and CeO_2 [52,53]. XPS analysis (Fig. 4d) of the Ce 3d shows that higher content of Ce^{3+} exists in the Pt/CeO_2-C, which is due to decreased crystalline sizes as confirmed by the XRD peak broadening (Fig. S3a, b). In combination with the curvature of the carbon layer, the defects promote the electron localization and increase the electron density [54]. Therefore, stronger EMSI can be achieved in the Pt/CeO_2-C. Meanwhile, CO-TPD (temperature programmed desorption) profiles of the as-prepared Pt/CeO_2 catalysts are comprised of two desorption peaks (Fig. S7) due to physically adsorbed CO and atop-bonded CO [55]. The desorption temperature of Pt/CeO_2-C is lower than that of Pt/CeO_2-P because CO chemisorption on the former is weakened, which suppresses the CO poisoning effect. Moreover, the strong EMSI between Pt and CeO_2 in the Pt/CeO_2-C is also evidenced by higher reduction temperature in hydrogen temperature programmed reduction (H_2-TPR) profiles (Fig. S8).

In situ DRIFTS

In situ diffuse reflectance infrared Fourier transform spectroscopy (*in situ* DRIFTS) studies were performed to understand the role of surface carbon on stabilizing the chemical states of CeO_2-supported Pt under reaction conditions because the chemical binding of CO is sensitive to both adsorption and local electronic structure of metal surfaces [26]. Fig. 5a shows two sets of IR peaks of the Pt/CeO_2-C catalysts that are centered at 2390–2310 and 2175–2120 cm^{-1}, attributed to gas phase CO_2 and CO, respectively [4]. And the IR peak of the adsorbed CO on metallic Pt^0 (at 2074 cm^{-1}, denoted as Pt^0-CO) [56] is weak due to the high reactivity of Pt at the measured temperature. The intensity of gas phase CO_2 adsorption increases with the reaction temperature, in agreement with increased CO conversion in Fig. 3. And the CO_2 intensity over Pt/CeO_2-C is much higher than that of Pt/CeO_2-P. The decay of catalytic activity for the Pt/CeO_2-P catalyst is also evidenced by the appearance of CO molecules residing on the catalyst surface as the reaction temperature increases to 90°C (Fig. 5b).

For the CO oxidation proceeding *via* CO adsorbed on Pt and CeO_2-activated O_2 [1,57], the reaction could be seriously suppressed if the interfacial Pt is oxidized due to over-stabilization of the surrounding lattice oxygen species bonded to the Pt atoms [26]. Using a photoemission

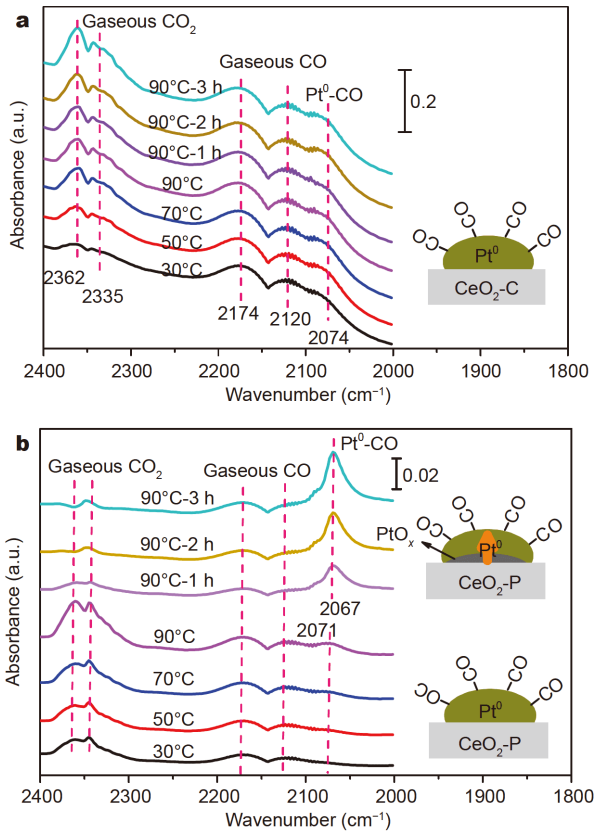

Figure 5 *In situ* DRIFTS of CO adsorbed on the Pt/CeO_2-C (a) and Pt/CeO_2-P (b) catalysts recorded under 1% CO, 20% O_2, and N_2 as balance.

electron microscopy (PEEM), Suchorshi *et al.* [3] found that the deactivation and reactivation of supported Pd particles were initiated at the perimeter sites and then expanded to further positions (Fig. 5b). In our previous study, we demonstrated that the spare charges due to interaction with support are not uniformly distributed and the getting/losing mainly occurs on the perimeter atoms of the metal NPs [17]. Therefore, it is reasonable to infer that the perimeter Pt atoms lose their valance electrons and get oxidized first during the decay process. Since the Pt-adsorbed CO cannot be eliminated by Ce^{3+}-activated O at the interface [57], the adsorbed CO molecules on metallic Pt^0 are observed on Pt/CeO_2-P. In contrast, no obvious IR peak related to Pt^0-CO is observed, suggesting that the valance electrons in Pt supported on graphitized CeO_2 is stabilized by the carbon so that its reactivity is maintained.

CONCLUSIONS

In conclusion, we have demonstrated a partially graphitized CeO_2 with porous structure as the support to stabilize the Pt NPs in both atomic and electronic structure.

Pt NPs are site-selectively grown on the carbon-ceria interface by surface redox reaction between Ce^{3+} and the Pt precursor. The carbonized porous CeO_2 was derived from Ce-BDC MOFs *via* pyrolysis in Ar. Benefiting from the unique structure of the three-phase junction of Pt-CeO_2-C, the Pt NPs exhibit enhanced activity and excellent stability for the CO oxidation by retaining their metallic Pt^0 states. Surface oxidation of metallic Pt^0 to $Pt^{\delta+}$ species on the CeO_2-P is the main reason for the deactivation in the investigated temperature range. The confinement effect of the interfacial carbon stabilizes the metallic Pt^0 state of the Pt NPs by promoting electron transfer from the support to the Pt NPs. The triple-junction strategy proposed in this work provides an additional dimension for precise adjustment of the metal-support interactions. With the assistance of the additional phase such as carbon, novel functional nanomaterials with outstanding performance could be constructed in the future.

Received 25 March 2020; accepted 16 April 2020; published online 10 July 2020

1 Nie L, Mei D, Xiong H, *et al.* Activation of surface lattice oxygen in single-atom Pt/CeO_2 for low-temperature CO oxidation. Science, 2017, 358: 1419–1423
2 Wang F, He S, Chen H, *et al.* Active site dependent reaction mechanism over Ru/CeO_2 catalyst toward CO_2 methanation. J Am Chem Soc, 2016, 138: 6298–6305
3 Suchorski Y, Kozlov SM, Bespalov I, *et al.* The role of metal/oxide interfaces for long-range metal particle activation during CO oxidation. Nat Mater, 2018, 17: 519–522
4 Chen G, Yang Y, Guo Z, *et al.* Thermally stable and highly active Pt/CeO_2@SiO_2 catalysts with a porous/hollow structure. Catal Sci Technol, 2018, 8: 4413–4419
5 Wang J, Xu M, Zhao J, *et al.* Anchoring ultrafine Pt electrocatalysts on TiO_2-C *via* photochemical strategy to enhance the stability and efficiency for oxygen reduction reaction. Appl Catal B-Environ, 2018, 237: 228–236
6 Cao XQ, Zhou J, Li S, *et al.* Ultra-stable metal nano-catalyst synthesis strategy: A perspective. Rare Met, 2020, 39: 113–130
7 Dai Y, Lu P, Cao Z, *et al.* The physical chemistry and materials science behind sinter-resistant catalysts. Chem Soc Rev, 2018, 47: 4314–4331
8 Campbell CT. The energetics of supported metal nanoparticles: Relationships to sintering rates and catalytic activity. Acc Chem Res, 2013, 46: 1712–1719
9 Chen J, Wanyan Y, Zeng J, *et al.* Surface engineering protocol to obtain an atomically dispersed Pt/CeO_2 catalyst with high activity and stability for CO oxidation. ACS Sustain Chem Eng, 2018, 6: 14054–14062
10 Hemmingson SL, Campbell CT. Trends in adhesion energies of metal nanoparticles on oxide surfaces: understanding support effects in catalysis and nanotechnology. ACS Nano, 2017, 11: 1196–1203
11 Cao X, Zhou J, Wang H, *et al.* Abnormal thermal stability of sub-10 nm Au nanoparticles and their high catalytic activity. J Mater Chem A, 2019, 7: 10980–10987
12 Chen G, Zhao Y, Fu G, *et al.* Interfacial effects in iron-nickel hydroxide-platinum nanoparticles enhance catalytic oxidation. Science, 2014, 344: 495–499
13 Cao K, Shi L, Gong M, *et al.* Nanofence stabilized platinum nanoparticles catalyst *via* facet-selective atomic layer deposition. Small, 2017, 13: 1700648
14 Zhang J, Wang L, Zhang B, *et al.* Sinter-resistant metal nanoparticle catalysts achieved by immobilization within zeolite crystals *via* seed-directed growth. Nat Catal, 2018, 1: 540–546
15 Liu H, Wang H, Liu Z, *et al.* Confinement impact for the dynamics of supported metal nanocatalyst. Small, 2018, 14: 1801586
16 Zhu X, Guo Q, Sun Y, *et al.* Optimising surface d charge of AuPd nanoalloy catalysts for enhanced catalytic activity. Nat Commun, 2019, 10: 1428
17 Liu Y, Chen H, Xu C, *et al.* Control of catalytic activity of nano-Au through tailoring the Fermi level of support. Small, 2019, 15: 1901789
18 Ahmadi M, Mistry H, Roldan Cuenya B. Tailoring the catalytic properties of metal nanoparticles *via* support interactions. J Phys Chem Lett, 2016, 7: 3519–3533
19 Bruix A, Rodriguez JA, Ramírez PJ, *et al.* A new type of strong metal-support interaction and the production of H_2 through the transformation of water on Pt/CeO_2 (111) and Pt/CeO_x/TiO_2 (110) catalysts. J Am Chem Soc, 2012, 134: 8968–8974
20 Campbell CT. Electronic perturbations. Nat Chem, 2012, 4: 597–598
21 Klyushin AY, Jones TE, Lunkenbein T, *et al.* Strong metal support interaction as a key factor of Au activation in CO oxidation. ChemCatChem, 2018, 10: 3985–3989
22 Xu C, Wu Y, Li S, *et al.* Engineering the epitaxial interface of Pt-CeO_2 by surface redox reaction guided nucleation for low temperature CO oxidation. J Mater Sci Tech, 2020, 40: 39–46
23 Tran SBT, Choi H, Oh S, *et al.* Defective Nb_2O_5-supported Pt catalysts for CO oxidation: promoting catalytic activity *via* oxygen vacancy engineering. J Catal, 2019, 375: 124–134
24 Lykhach Y, Kozlov SM, Skála T, *et al.* Counting electrons on supported nanoparticles. Nat Mater, 2016, 15: 284–288
25 Kim GJ, Kwon DW, Hong SC. Effect of Pt particle size and valence state on the performance of Pt/TiO_2 catalysts for CO oxidation at room temperature. J Phys Chem C, 2016, 120: 17996–18004
26 Ke J, Zhu W, Jiang Y, *et al.* Strong local coordination structure effects on subnanometer PtO_x clusters over CeO_2 nanowires probed by low-temperature CO oxidation. ACS Catal, 2015, 5: 5164–5173
27 Vayssilov GN, Lykhach Y, Migani A, *et al.* Support nanostructure boosts oxygen transfer to catalytically active platinum nanoparticles. Nat Mater, 2011, 10: 310–315
28 Lu G, Hupp JT. Metal-organic frameworks as sensors: A ZIF-8 based Fabry-Perot device as a selective sensor for chemical vapors and gases. J Am Chem Soc, 2010, 132: 7832–7833
29 Rong J, Qiu F, Zhang T, *et al.* Non-noble metal@carbon nanosheet derived from exfoliated MOF crystal as highly reactive and stable heterogeneous catalyst. Appl Surf Sci, 2018, 447: 222–234
30 Horcajada P, Chalati T, Serre C, *et al.* Porous metal-organic-framework nanoscale carriers as a potential platform for drug delivery and imaging. Nat Mater, 2010, 9: 172–178
31 Zhang P, Chen C, Kang X, *et al. In situ* synthesis of sub-nanometer metal particles on hierarchically porous metal-organic frameworks *via* interfacial control for highly efficient catalysis. Chem Sci, 2018,

9: 1339–1343
32 deKrafft KE, Wang C, Lin W. Metal-organic framework templated synthesis of Fe_2O_3/TiO_2 nanocomposite for hydrogen production. Adv Mater, 2012, 24: 2014–2018
33 Kaneti YV, Dutta S, Hossain MSA, *et al.* Strategies for improving the functionality of zeolitic imidazolate frameworks: Tailoring nanoarchitectures for functional applications. Adv Mater, 2017, 29: 1700213
34 Bai X, Chen D, Li L, *et al.* Fabrication of MOF thin films at miscible liquid-liquid interface by spray method. ACS Appl Mater Interfaces, 2018, 10: 25960–25966
35 Kaneti YV, Zhang J, He YB, *et al.* Fabrication of an MOF-derived heteroatom-doped Co/CoO/carbon hybrid with superior sodium storage performance for sodium-ion batteries. J Mater Chem A, 2017, 5: 15356–15366
36 Tang J, Salunkhe RR, Zhang H, *et al.* Bimetallic metal-organic frameworks for controlled catalytic graphitization of nanoporous carbons. Sci Rep, 2016, 6: 30295
37 Nguyen CC, Nguyen DT, Do TO. A novel route to synthesize C/Pt/TiO_2 phase tunable anatase-rutile TiO_2 for efficient sunlight-driven photocatalytic applications. Appl Catal B-Environ, 2018, 226: 46–52
38 Ning X, Li Y, Dong B, *et al.* Electron transfer dependent catalysis of Pt on N-doped carbon nanotubes: Effects of synthesis method on metal-support interaction. J Catal, 2017, 348: 100–109
39 Isaeva VI, Belyaeva EV, Fitch AN, *et al.* Synthesis and structural characterization of a series of novel Zn(II)-based MOFs with pyridine-2,5-dicarboxylate linkers. Cryst Growth Des, 2013, 13: 5305–5315
40 Zhao P, Qin F, Huang Z, *et al.* MOF-derived hollow porous Ni/CeO_2 octahedron with high efficiency for N_2O decomposition. Chem Eng J, 2018, 349: 72–81
41 Cao F, Zhang S, Gao W, *et al.* Facile synthesis of highly-dispersed Pt/CeO_2 by a spontaneous surface redox chemical reaction for CO oxidation. Catal Sci Technol, 2018, 8: 3233–3237
42 Liu H, Wang J, Feng Z, *et al.* Facile synthesis of Au nanoparticles embedded in an ultrathin hollow graphene nanoshell with robust catalytic performance. Small, 2015, 11: 5059–5064
43 Li WZ, Kovarik L, Mei D, *et al.* Stable platinum nanoparticles on specific $MgAl_2O_4$ spinel facets at high temperatures in oxidizing atmospheres. Nat Commun, 2013, 4: 2481
44 Ouyang R, Liu JX, Li WX. Atomistic theory of ostwald ripening and disintegration of supported metal particles under reaction conditions. J Am Chem Soc, 2013, 135: 1760–1771
45 Naumann d'Alnoncourt R, Friedrich M, Kunkes E, *et al.* Strong metal-support interactions between palladium and iron oxide and their effect on CO oxidation. J Catal, 2014, 317: 220–228
46 Yu X, Wang Y, Kim A, *et al.* Observation of temperature-dependent kinetics for catalytic CO oxidation over TiO_2-supported Pt catalysts. Chem Phys Lett, 2017, 685: 282–287
47 Gracia FJ, Bollmann L, Wolf EE, *et al. In situ* FTIR, EXAFS, and activity studies of the effect of crystallite size on silica-supported Pt oxidation catalysts. J Catal, 2003, 220: 382–391
48 Bera P, Priolkar KR, Gayen A, *et al.* Ionic dispersion of Pt over CeO_2 by the combustion method: structural investigation by XRD, TEM, XPS, and EXAFS. Chem Mater, 2003, 15: 2049–2060
49 Liu J, Ding T, Zhang H, *et al.* Engineering surface defects and metal-support interactions on Pt/TiO_2 (B) nanobelts to boost the catalytic oxidation of CO. Catal Sci Technol, 2018, 8: 4934–4944
50 Li QQ, Zhang X, Han WP, *et al.* Raman spectroscopy at the edges of multilayer graphene. Carbon, 2015, 85: 221–224
51 Fu Y, Yu HY, Jiang C, *et al.* NiCo alloy nanoparticles decorated on N-doped carbon nanofibers as highly active and durable oxygen electrocatalyst. Adv Funct Mater, 2018, 28: 1705094
52 Liu J, Yue Y, Liu H, *et al.* Origin of the robust catalytic performance of nanodiamond-graphene-supported Pt nanoparticles used in the propane dehydrogenation reaction. ACS Catal, 2017, 7: 3349–3355
53 Jia Z, Huang F, Diao J, *et al.* Pt NPs immobilized on a N-doped graphene@Al_2O_3 hybrid support as robust catalysts for low temperature CO oxidation. Chem Commun, 2018, 54: 11168–11171
54 Sun X, Wang R, Zhang B, *et al.* Evolution and reactivity of active oxygen species on sp^2@sp^3 core-shell carbon for the oxidative dehydrogenation reaction. ChemCatChem, 2014, 6: 2270–2275
55 Padilla R, Benito M, Rodríguez L, *et al.* Platinum supported catalysts for carbon monoxide preferential oxidation: Study of support influence. J Power Sources, 2009, 192: 114–119
56 Jardim EO, Rico-Francés S, Coloma F, *et al.* Influence of the metal precursor on the catalytic behavior of Pt/ceria catalysts in the preferential oxidation of CO in the presence of H_2 (PROX). J Colloid Interface Sci, 2015, 443: 45–55
57 Kopelent R, van Bokhoven JA, Szlachetko J, *et al.* Catalytically active and spectator Ce^{3+} in ceria-supported metal catalysts. Angew Chem Int Ed, 2015, 54: 8728–8731

Acknowledgements This work was supported by the National Key Research and Development Program of China (2016YFB0701100), the National Natural Science Foundation of China (51771047, 51525101 and 51971059), and the Fundamental Research Funds for the Central Universities (N180204014).

Author contributions Li S and Xu C conceived the idea and designed the experiments. Xu C, Zhang Y, and Chen J carried out the synthesis, characterization and catalytic experiments. All authors contributed to the discussion of the results and commented on the manuscript writing.

Conflict of interest The authors declare that they have no conflict of interest.

Supplementary information Experimental details and supporting data are available in the online version of the paper.

Changjin Xu received his BSc degree from Inner Mongolia Agricultural University in 2014. Currently, he is a PhD student in the School of Materials Science and Engineering at Northeastern University (China). His research interests focus on the heterogeneous nanocatalysts.

Song Li is a professor of materials science and engineering at Northeastern University, China. He received his BSc degree in 2003 from Northeastern University and PhD degree in materials physics from the University of Lorraine in 2009. His current research focuses on metal-based structured catalysts, including noble metal alloys and intermetallics, metal-oxide interfaces, and processing intensification.

碳-CeO_2界面增强Pt纳米催化剂在催化氧化反应中的化学稳定性

徐长进[1], 张钺[1], 陈晶[2], 李松[1*], 张亚文[3], 秦高梧[1,4]

摘要 为提高贵金属催化剂的活性与原子经济性, 人们将其粒径降低至纳米/亚纳米尺度, 甚至开发各类单原子材料. 然而, 这些材料的结构状态和催化性能难以在苛刻的催化环境下保持稳定. 对于二氧化铈(CeO_2)负载的Pt纳米粒子, 载体扩散到Pt粒子表面的活性氧物种稳定吸附在Pt表面, 导致金属Pt活性降低. 本文采用表面部分碳修饰的多孔CeO_2为载体, 将纳米Pt选择性地生长在C-CeO_2界面处形成特殊的三相界面结构, 对CO氧化表现出低温段增强的活性和稳定性. 石墨碳对纳米Pt的供电子效应和CeO_2载体高密度纳米孔的限域效应共同贡献了纳米Pt的化学及结构稳定性. 本文设计的独特三相界面结构综合了CeO_2活化氧以及碳贡献电子能力的优点, 为制备新型高效金属催化材料提供了新的思路.